IEEE Access
Multidisciplinary | Rapid Review | Open Access Journal

Received December 15, 2018, accepted January 13, 2019, date of publication January 21, 2019, date of current version February 6, 2019.

Digital Object Identifier 10.1109/ACCESS.2019.2893449

Modeling of Lightning Transients in Photovoltaic Bracket Systems

YAOWU WANG, XIAOQING ZHANG, AND SHIQI TAO
School of Electrical Engineering, Beijing Jiaotong University, Beijing 100044, China
Corresponding author: Yaowu Wang (16117407@bjtu.edu.cn)

This work was supported by the National Natural Science Foundation of China under Grant 51777007.

ABSTRACT The lightning transient calculation is carried out in this paper for photovoltaic (PV) bracket systems. The electrical parameters of the conducting branches and earthing electrodes are represented by resistances, capacitances, and inductances. A set of formulas are derived to evaluate the electrical parameters, which are appropriate for the complicated spatial locations of the conducting branches. On the basis of the electrical parameters, the equivalent circuits are constructed for the segmented branches and electrode units in a PV bracket system. By integrating all the equivalent circuits, a complete circuit model is built for the PV bracket system. The lightning transient responses can be obtained from the circuit model. In order to confirm the validity of the circuit model, experimental measurement is made with a reduced-scale PV bracket system and the measured results are compared with the calculated ones. Then, an actual PV bracket system is used as the numerical example. The lightning transient responses are calculated for typical locations of attachment points. The distribution characteristic of lightning transient responses is also explored in the PV bracket system.

INDEX TERMS Modeling, lightning transient, photovoltaic, bracket system, lightning protection.

I. INTRODUCTION

With a rapid growth in photovoltaic power generation, lightning hazard to PV installations has come to be regarded with much attention. PV installations are vulnerable to lightning stroke owing to their expended surface and exposed location. When the metal supporting framework of solar panel is struck by lightning, a high impulse current flows through various conducting branches in the bracket system and dissipates from the earthing arrangement into the ground. During this transient travelling process, the lightning current will generate overheat and overvoltage surges in the bracket system and does damage to the supporting framework and other PV components. The associated damage events and related costs have been reported in [1]–[4]. Therefore, it is necessary to perform lightning transient analysis for bracket systems. Knowledge of the transient responses in the bracket systems can provide a valuable support for lightning protection design of PV installations. Up to now, research efforts have been untaken to lightning protection of PV installations. The laboratory and field measurements were made for the performance of lightning stroke to PV installations [5]–[8]. The numerical calculations were also performed in exploring the induced overvoltage behavior in solar panels and arrays [9]–[11]. However, a systematic research on the lightning transient modeling of the bracket systems has not been found in the literature. There has been a lack of the available results for the distribution characteristic of lightning transient responses in the bracket systems. This is difficult to fulfill the practical requirement of lightning protection design of PV installations. Considering the imperfection of the previous work, a modeling method is proposed in this paper for calculating the lightning transients in the bracket system. In the method, a set of formulas are deduced for evaluating the electrical parameters of the conducting branches in the bracket systems. On the basis of the electrical parameters, the circuit model is built for the bracket systems. The lightning transient responses in the bracket systems can be obtained by using the circuit model to perform the transient calculation. A laboratory experiment is made on a reduced-scale bracket system and the measured results are employed to check the validity of the circuit model. Additionally, an investigation is also made on the distribution of lightning transient responses in an actual bracket system.

II. ELECTRICAL PARAMETERS

A PV bracket system is diagrammatically illustrated in Fig. 1. It mainly comprises the supporting framework above the earth surface and foundation earthing arrangement. The former

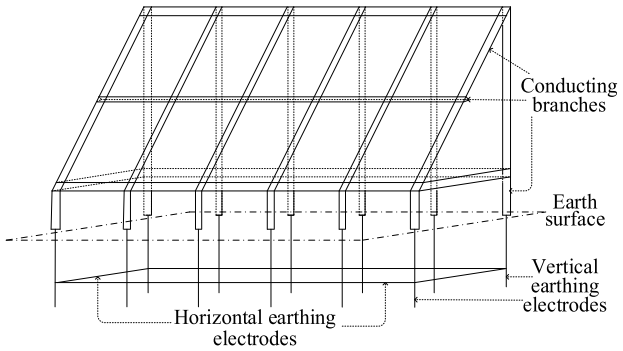

FIGURE 1. PV bracket system structure.

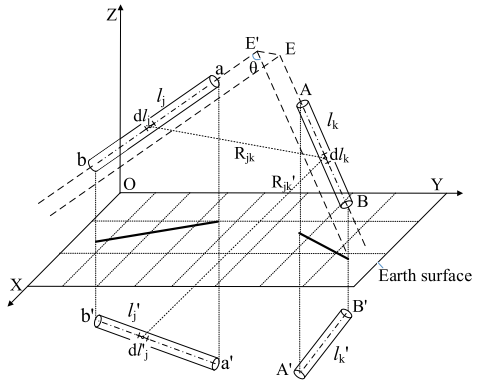

FIGURE 2. Non-parallel conductors.

is composed of the conducting branches in different spatial positions and the latter of the horizontal and vertical electrodes buried underground. The circuit parameters of the conducting branches and earthing electrodes are represented by resistances, capacitances and inductances. Due to the fact that electromagnetic couplings among the conducting branches, the capacitances and inductances take the form of their respective matrixes. The formulas for evaluating these circuit parameters are derived respectively in the following.

A. CONDUCTING BRANCHES

1) CAPACITANCES PARAMETERS

For the sake of simplification, a conducting branch in the supporting framework is equivalently taken as a cylindrical conductor with its radius estimated from the branch cross-section [12], [13]. To evaluate the capacitances of the conducting branches, the corresponding potential coefficients need to be determined in advance. According to the relative spatial positions of the conducting branches shown in Fig. 1, the branch pairs may be geometrically classified into three kinds of positional relationships, i. e. non-parallel and parallel branch pairs. Their potential coefficients can be evaluated by the mean potential integral [14] and the presence of the ground is taken into account by the image method [14] and [15].

For a non-coplanar branch pair, namely branches j and k, as shown in Fig. 2, its imaginary branches are installed at the symmetrical position below the earth surface and depicted by the dotted lines [14]. The mutual potential coefficient between the two branches is calculated by [15].

$$P_{jk} = (\Lambda_{jk} - \Lambda'_{jk})/4\pi\varepsilon l_j l_k \tag{1}$$

where Λ_{jk} and Λ'_{jk} are the double line integrals

$$\begin{aligned}\Lambda_{jk} &= \int_{l_j}\int_{l_k} \left(1/R_{jk}\right) dl_k dl_j \\ \Lambda'_{jk} &= \int_{l'_j}\int_{lk} \left(1/R'_{jk}\right) dl_k dl'_j\end{aligned} \tag{2}$$

According to the spatial position dimensions of the branches j and k, Λ_{jk} is given by

$$\begin{aligned}\Lambda_{jk} &= \int_{l_k}\int_{l_j} 1/R_{jk} dl_j dl_k \\ &= (d_2 + l_j)\ln\left[(d_4 + d_5 + l_k)/(d_4 + d_5 - l_k)\right] \\ &\quad - d_2\ln\left[(d_6 + d_7 + l_k)/(d_6 + d_7 - l_k)\right] \\ &\quad + (d_3 + l_k)\ln\left[(d_4 + d_7 + l_j)/(d_4 + d_7 - l_j)\right] \\ &\quad - d_3\ln\left[(d_5 + d_6 + l_j)/(d_5 + d_6 - l_j)\right] - \delta d/\sin\theta\end{aligned} \tag{3}$$

where the solid angle δ is

$$\begin{aligned}\delta &= \tan^{-1}[d_1/d_4\tan\theta + (d_2 + l_j)(d_3 + l_k)\sin\theta/d_1 d_4] \\ &\quad - \tan^{-1}[d_1/d_5\tan\theta + (d_2 + l_j)d_3\sin\theta/d_1 d_5] \\ &\quad + \tan^{-1}[d_1/d_6\tan\theta + d_2 d_3\sin\theta/d_1 d_6] \\ &\quad - \tan^{-1}[d_1/d_7\tan\theta + d_2(d_3 + l_k)\sin\theta/d_1 d_7]\end{aligned} \tag{4}$$

where d_1, d_2, d_3, d_4, d_5, d_6, d_7 are the lengths of lines E'E, EA, E'a, Bb, Ba, Aa, Ab (see Fig. 2), respectively.

If $\theta = \pi/2$ and $\delta d/\sin\theta \neq 0$, (3) represents the integral formula of a perpendicular non-coplane branch pair.

In the coplane situation, the corresponding formulas can also be obtained by setting $d_1 = 0$ into (3). If $\theta \neq \pi/2$, (3) gives the integral formula of a non-perpendicular coplane branch pair. As a special case, the integral formula of a perpendicular coplane branch pair is obtained by setting $\theta = \pi/2$ into (3).

Since the way of evaluating Λ'_{jk} is same as that of evaluating Λ_{jk}, Λ'_{jk} can be given in a similar integral formula. Due to the limit of length, the integral formula of Λ'_{jk} is omitted.

For a parallel branch pair, i.e. branches m and n, as shown in Fig 3, its double integral Λ_{mn} is evaluated by

$$\begin{aligned}\Lambda_{mn} &= \int_{l_m}\int_{l_n} 1/R_{mn} dl_m dl_n \\ &= (l_m + d_9 + l_n)\sinh^{-1}(l_m + d_9 + l_n/d_8) \\ &\quad - \sqrt{(l_m + d_9 + l_n)^2 + d_8^2} + d_9\sinh^{-1}(d_9/d_8) \\ &\quad - \sqrt{d_8^2 + d_9^2} - (m + d_9)\sinh^{-1}(l_n + d_9/d_8) \\ &\quad + \sqrt{(l_n + d_9)^2 + d_8^2} \\ &\quad - (l_m + d_9)\sinh^{-1}(l_m + d_9/d_8) + \sqrt{(l_m + d_9)^2 + d_8^2}\end{aligned} \tag{5}$$

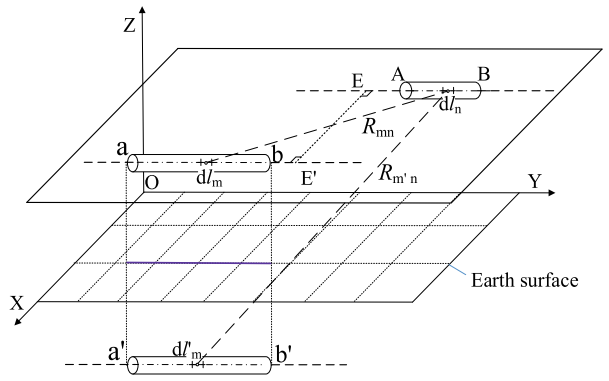

FIGURE 3. Parallel conducting branch pair.

where d8 and d9 are the lengths of lines EE′ and AE, respectively.

In Fig. 2 or Fig. 3, letting the axial of branch k or branch n coincide with the generatrix of branch j or branch m, the double integral Λ_{jj} or Λ_{mm} is evaluated. Consequently, the self potential coefficient p_{jj} or p_{mm} can be obtained.

On the basis of the self and mutual potential coefficients, the potential matrix $\boldsymbol{P}$ for N coupled branches is represented by

$$\boldsymbol{P} = \begin{bmatrix} p_{11} & p_{12} & \cdots & p_{1N} \\ p_{21} & p_{22} & \cdots & p_{2N} \\ \vdots & \vdots & \ddots & \vdots \\ p_{N1} & p_{N2} & \cdots & p_{NN} \end{bmatrix} \tag{6}$$

The inverse of $\boldsymbol{P}$ is represented by

$$\boldsymbol{Q} = \boldsymbol{P}^{-1} = \begin{bmatrix} q_{11} & q_{12} & \cdots & q_{1N} \\ q_{21} & q_{22} & \cdots & q_{2N} \\ \vdots & \vdots & \ddots & \vdots \\ q_{N1} & q_{N2} & \cdots & q_{NN} \end{bmatrix} \tag{7}$$

In terms of $\boldsymbol{Q}$, the capacitance matrix is formed by

$$\boldsymbol{C} = \begin{bmatrix} C_{11} & C_{12} & \cdots & C_{1N} \\ C_{21} & C_{22} & \cdots & C_{2N} \\ \vdots & \vdots & \ddots & \vdots \\ C_{N1} & C_{N2} & \cdots & C_{NN} \end{bmatrix} \tag{8}$$

The self and mutual capacitance elements in $\boldsymbol{C}$ are determined as follows

$$\begin{aligned} C_{jj} &= \sum_{j=1}^{N} p'_{jk} \quad (j = 1, 2, \ldots, N) \\ C_{jj} &= -p'_{jk} \quad (j, k = 1, 2, \ldots N, k \neq j) \end{aligned} \tag{9}$$

2) INDUCTANCE AND RESISTANCE PARAMETERS

According to the Neumann's formula, the branch inductance matrix L can be calculated by [14], [16]

$$\boldsymbol{L} = \boldsymbol{P} \times \mu_0/4\pi \tag{10}$$

The resistance matrix R of N branches is a diagonal matrix, namely

$$\boldsymbol{R} = \mathrm{diag}[R_1, R_2, \ldots, R_N] \tag{11}$$

where the resistance Rj (j = 1, 2, ···, N) is estimated by [17]

$$R_j = \sqrt{\mu f_c}/(2r_0\sqrt{\pi\sigma}) \tag{12}$$

where μ, σ and r_0 are the permeability(H/m), conductivity(S · m^{-1}) and radius of the branch(m), respectively. f_c is the maximum frequency(hz) likely to affect the system transient and may be roughly evaluated by the waveform parameters of the injected lightning current [18].

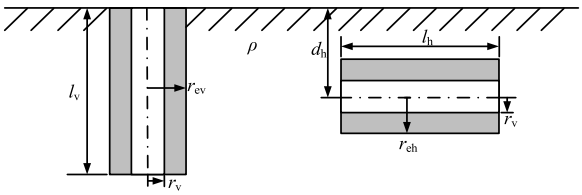

FIGURE 4. Equivalent radii of vertical and horizontal earthing electrodes.

B. EARTHING ARRANGEMENT

When a lightning current dissipates into the ground though an earthing electrode, the high electric field intensity occurs near the earthing electrode and results in the soil breakdown here. This can be regarded as an increase in the radius of the earthing electrode, as illustrated in Fig. 4. For the vertical and horizontal earthing electrodes, their equivalent radii including the soil breakdown are estimated by [19].

$$r_v = 1/2\big(-l_v + \sqrt{l_v^2 + 2\rho i_v/\pi E_0}\big) \tag{13}$$

$$r_h = \rho i_h/2\pi l_h E_0 \tag{14}$$

where ρ is the soil resistivity(Ω·m), E_0 is the critical breakdown field intensity of the soil(V/m).

Due to the fact that the horizontal dimension of the bracket system is rather large, the length of the horizontal earthing electrode is far longer than that of the vertical earthing electrode. Therefore, the distribution parameter effect should be considered for the horizontal earthing electrode. Its capacitance and inductance are evaluated by [20].

$$C_h = 2\pi\varepsilon l_h/[\ln(2\rho/\sqrt{2d_h r_h}) - 1] \tag{15}$$

$$L_h = [\ln(2\rho/\sqrt{2d_h r_h}) - 1]\mu_0 l_h/2\pi \tag{16}$$

$$G_h = 2\pi/\rho[\ln(2l_h/\sqrt{2r_h d_h}) - 1] \tag{17}$$

where ε is the permittivity of the soil(F/m).

In consideration of a shorter length, the circuit parameter of the vertical earthing electrode is only represented by an impulse earthing resistance [17].

$$\begin{aligned} R_{iv} &= \rho\ln(2l_v/r_{ev} + 1)/2\pi l_v \quad r_{ev} < 0.4l_v \\ R_{iv} &= \rho\ln(\sqrt{l_v^2 + r_{ev}^2} + l_v/r_{ev})/2\pi l_v \quad 0.4l_v < r_{ev} < l_v \end{aligned} \tag{18}$$

III. EQUIVALENT CIRCUIT MODEL

In order to take the traveling wave behavior of lightning current into account, the conducting branches and horizontal earthing electrodes need to be divided into a reasonable number of segments. The length of each segment is shorter than the 1/10 of c/f_c [21], where c is the velocity of light. On the basis of the circuit parameters, M coupled segments in the supporting framework can be represented by a coupled π-type circuit unit formed by resistances, inductances and capacitances. The coupled π-type circuit unit representing two coupled branches (M = 2) is shown in Fig. 5.

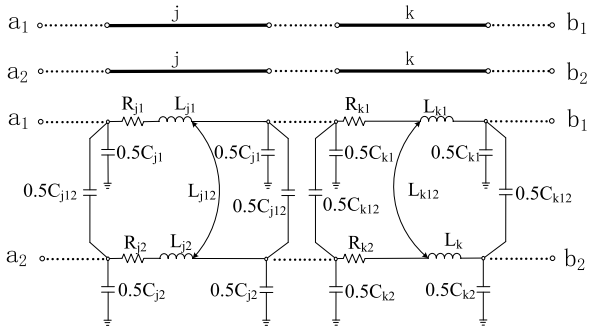

FIGURE 5. PV framework equal π style coupled circuits.

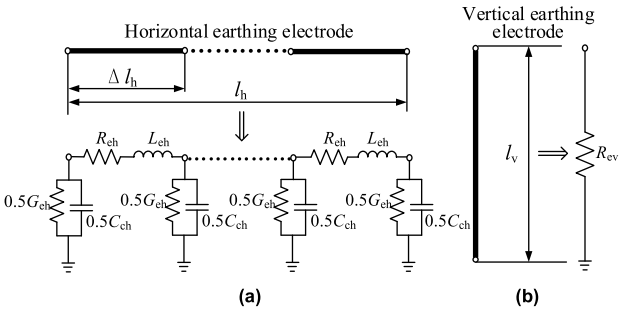

FIGURE 6. Grounding conductors equal π style circuits.

For an actual PV earthing arrangement, the horizontal earthing electrode, due to its great length, needs be divided into a number of segments. Each horizontal segment is represented by a π-type circuit, as shown in Fig. 6 (a). However, the length of the vertical earthing electrode is usually short (1.5 m$\sim$2 m). The vertical earthing electrode is represented by a lumped impulse earthing resistance for the sake of simplicity, as shown in Fig. 6 (b).

Subsequent to obtaining the equivalent circuits of conducting branches and earthing electrodes, the bracket system is converted into a large scale electrical network formed by resistances, capacitances and inductances, as shown Fig. 7. The lightning stroke to the supporting framework is simulated by a lightning current source is injected to the node corresponding to the attachment point. The impedance Z in parallel with is the surge impedance of the lightning channel. The estimate values of Z from limited experimental and computed data range from several hundred ohms to a few kiloohms [22].

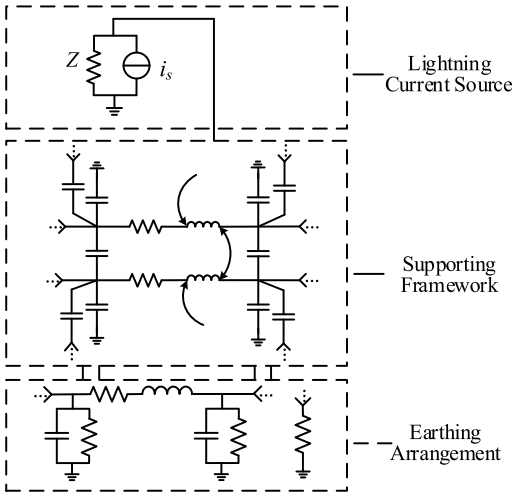

FIGURE 7. Equivalent electrical network of PV bracket system.

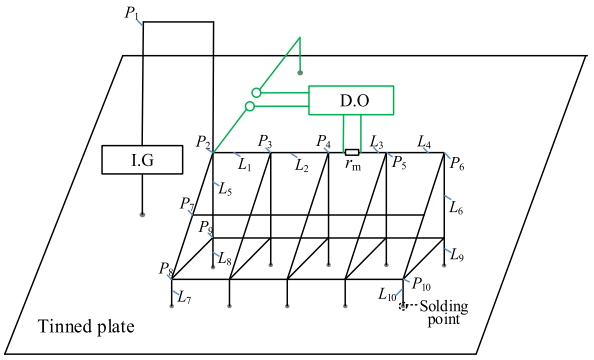

FIGURE 8. Experiment setup (I.G—impluse generator, D.O—digital oscilloscope, r_m—non-inductive resistance).

Following a time discretization treatment for the capacitances and series resistance-inductances, these two kinds of circuit elements are replaced by current sources and parallel equivalent resistances. Thus, Fig. 7 is further converted into an equivalent network only composed of current sources and resistances. The node voltage equations are set up for the equivalent network and the lightning transient responses can be computed by numerically solving the equations. The detailed algorithm has been presented in [23].

IV. EXPERIMENTAL MEASUREMENT

A. CONDUCTING BRANCHES

An experimental setup is built to measure the transient responses in a reduced-scale bracket system, as illustrated in Fig. 8. In the experimental setup, the impulse generator consists of resistor, capacitor, inductor and dc source, as shown in Figs. 9(a) and (b). To take into account the distribution parameter behavior of lightning transients in the actual bracket system, the fast impulse current is regulated to a short wavefront time with tens of nanoseconds and its waveform is shown in Fig. 9(c). The reduced-scale bracket system is made of the steel bars with a diameter of 5 mm, as shown

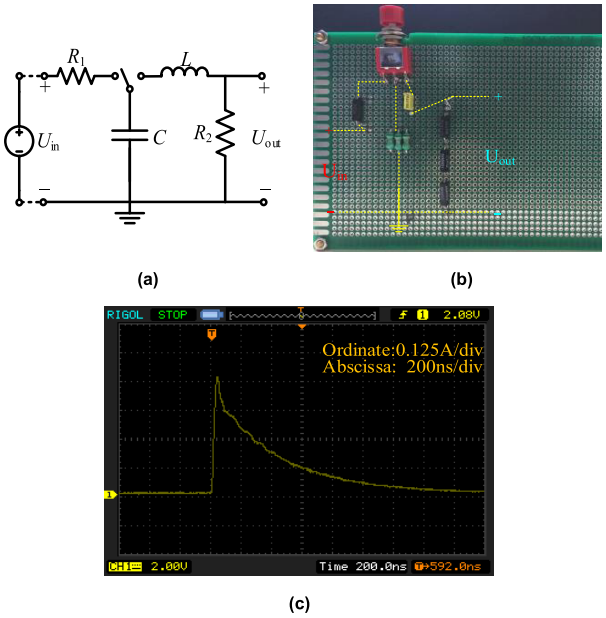

FIGURE 9. Impulse generator. (a) Circuit diagram. (b) Circuit board. (c) Impulse current waveform.

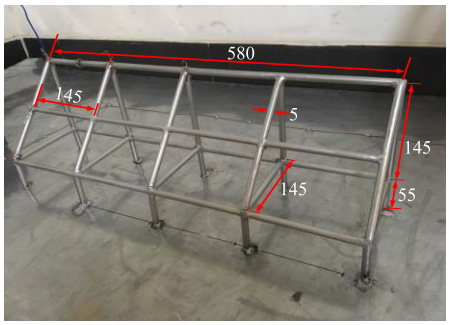

FIGURE 10. Reduced-scale PV framework model, unit(mm).

TABLE 1. Measured and calculated peak potentials.

Node	Calculated Value(V)	Measured Value(V)
P1	20.85	21
P2	13.50	14.4
P3	12.12	13.4
P4	11.93	13.1
P5	11.92	13
P6	11.92	12.8
P7	12.63	13.5
P8	12.28	13.5
P9	12.31	13.6
P10	11.91	12.1

in Fig. 10, and its sizes are also marked here. The currents are measured by the non-inductive resistors rm The reference potential point for potential measurement is connected to the tinplate(do not consider soil ionization effect in reduced-scale experiment) at a point 5 m apart from the reduced-scale bracket system, where an approximate electrical null is provided. The measurement wires for the potential and

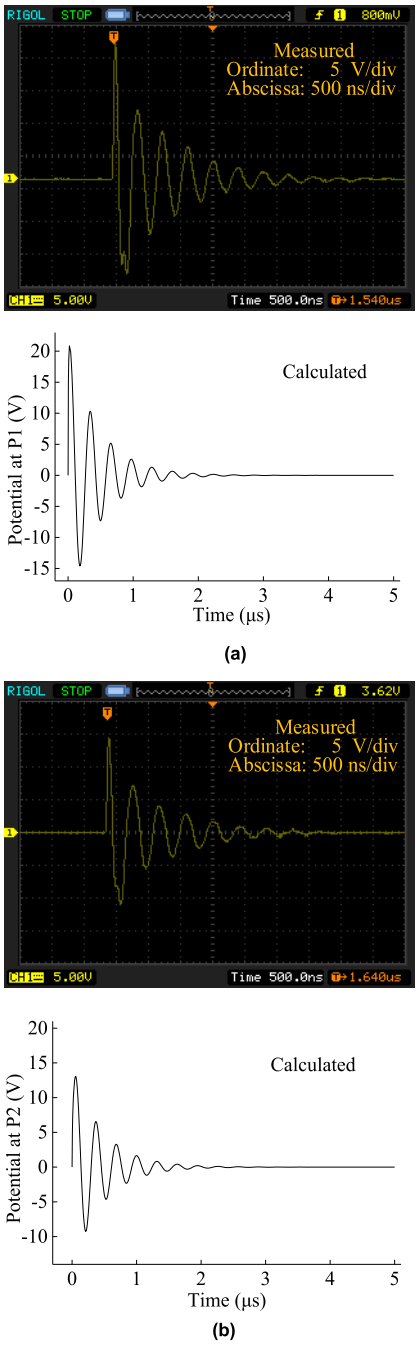

FIGURE 11. Measured and calculated Potential waveforms. (a) Potential waveforms at P1. (b) Potential waveforms at P2.

current are stretched perpendicular to the current lead wire from the impulse generator for reducing the electromagnetic induction between them. The current and potential signals are recorded by a digital oscilloscope with a frequency bandwidth of 200 MHz.

B. MEASURED RESULTS

The measured peak potentials at nodes P1 P10 are given in Table 1 and the measured potential waveforms at nodes P1 and P2 are shown in Fig. 11. Moreover, the measured

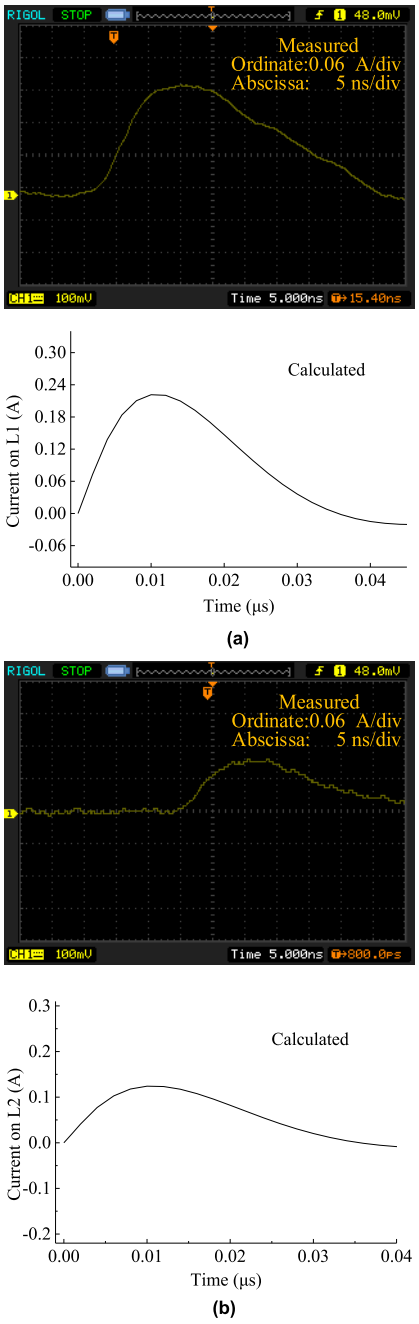

FIGURE 12. Measured and calculated Current waveforms. (a) Measured and calculated current waveforms on branch L1. (b) Measured and calculated current waveforms on branch L2.

peak currents on branches L1 ∼ L2 are given in Table 2 and the measured current waveforms on branches L1 ∼ L2 are shown in Fig. 12. For the sake of comparison, the corresponding results calculated by the equivalent circuit model proposed above are simultaneously given in Tables 1 ∼ 2 and Figs.11 ∼ 12. As can be seen from the comparison that a better agreement appears between the measured and calculated results, which confirms the validity of the circuit model.

TABLE 2. Measured and calculated peak currents.

Node	Calculated Value(A)	Measured Value(A)
L1	0.23	0.22
L2	0.11	0.10
L3	0.056	0.06
L4	0.027	0.03
L5	0.19	0.20
L6	0.024	0.03
L7	0.071	0.07
L8	0.072	0.07
L9	0.056	0.06
L10	0.056	0.06

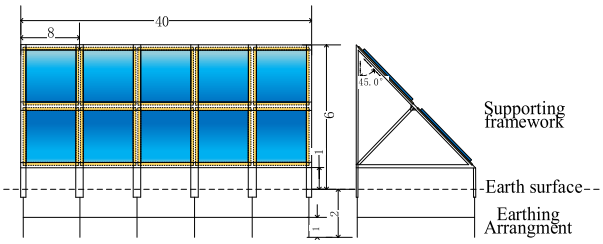

FIGURE 13. PV bracket system numerical example, unit (m).

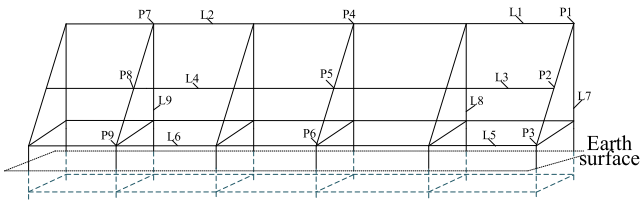

FIGURE 14. PV system lightning transient simulation experiment diagrammatic drawing.

V. NUMERICAL EXAMPLE

A. CALCULATION CONDITIONS

An actual PV bracket system is taken into account in this numerical example and its dimensions are illustrated in Fig. 13. In the transient calculation, Fig. 13 is converted into an equivalent conductor structure, as shown in Fig. 14. The waveform parameters of lightning current source are taken as 10/350 μs and 100 kA according to the lightning protection design specifications [24]. The soil resistivity ρ is 200 Ω·m and a uniform soil condition is considered here for the purpose of engineering application. In Fig. 14, the typical nodes and branches are marked by P1∼P9 and L1∼L9, respectively.

B. CALCULATED RESULTS AND DISCUSSION

The node P1 in the roof corner is first taken as the attachment point, since it is easy to strike by lightning. The calculated waveforms of transient potentials and currents are depicted in Figs. 15∼16, respectively.

As can be seen from Fig. 15 that the evident oscillations appear on the potential waveforms. The oscillation phenomenon is caused by a large number of capacitances and

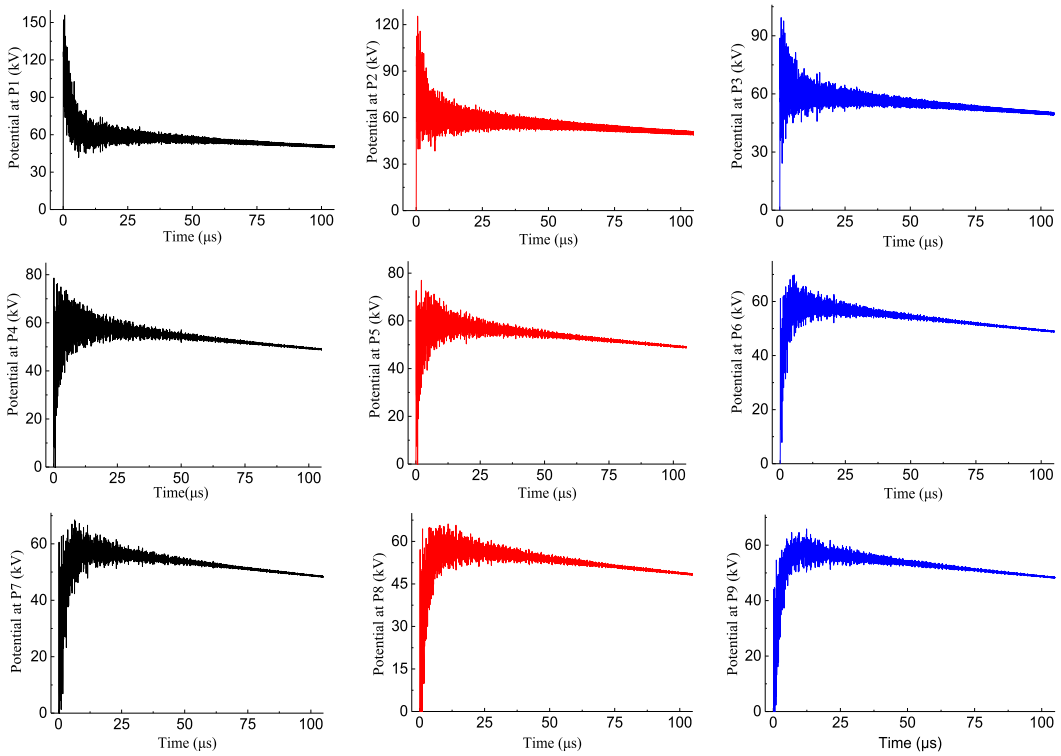

FIGURE 15. Potential waveforms.

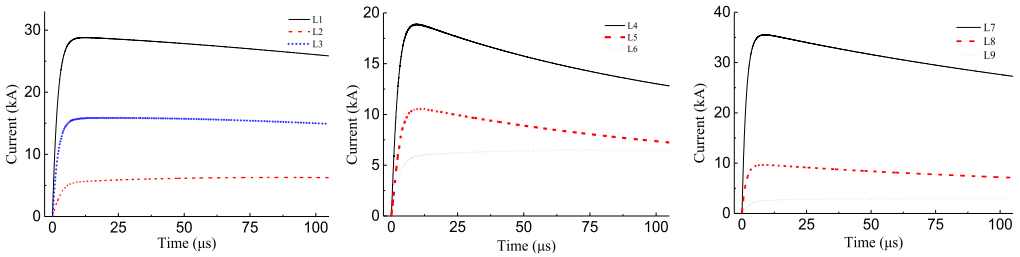

FIGURE 16. Current waveforms.

inductances in the equivalent electrical network of the bracket system. The peak potential attains a maximum value at the attachment point P1 and gradually decrease with an increase in the distance from P1. On the other hand, the branch currents close to P1 are also significantly higher than those distant from P1, as indicated in Fig. 16. In general, the transient responses in the supporting framework exhibit a tendency to weaken with the distance from the attachment point. The reason for this is mainly that the various branches perform the function of current-division when the injected lightning current flows to the ground along different paths.

For dynamically examining the distribution behavior of the lightning transient responses in the supporting framework, the instantaneous values of the currents and potentials are extracted from at three typical instants of the transient process, i.e. t = 0.55 μs, 10 μs and 350 μs. The instantaneous current factor (ICF) is defined as the ratio of instantaneous branch current to instantaneous lightning current and its distribution is illustrated in Fig. 17. It can be seen from Figs. 17(a) and (b) that ICFs take quite great values on the branches connected with the attachment point, while they are quite low on the branches distant from the attachment point. Therefore, the current distribution in the supporting framework exhibits a high non-uniform degree, which indicates that the current distribution mainly concentrates on the branches close to the attachment point at the initial stage of the transient process, i.e. t = 0.55 μs $\sim$ 10 μs. With the development of the transient process, the distortion degree of the current distribution decreases to a certain extent. ICFs on the vertical branches at the bottom of the supporting framework are approximately equal to each other at t = 350 μs, as shown in Fig. 18(c). However, ICFs on the branches connected with

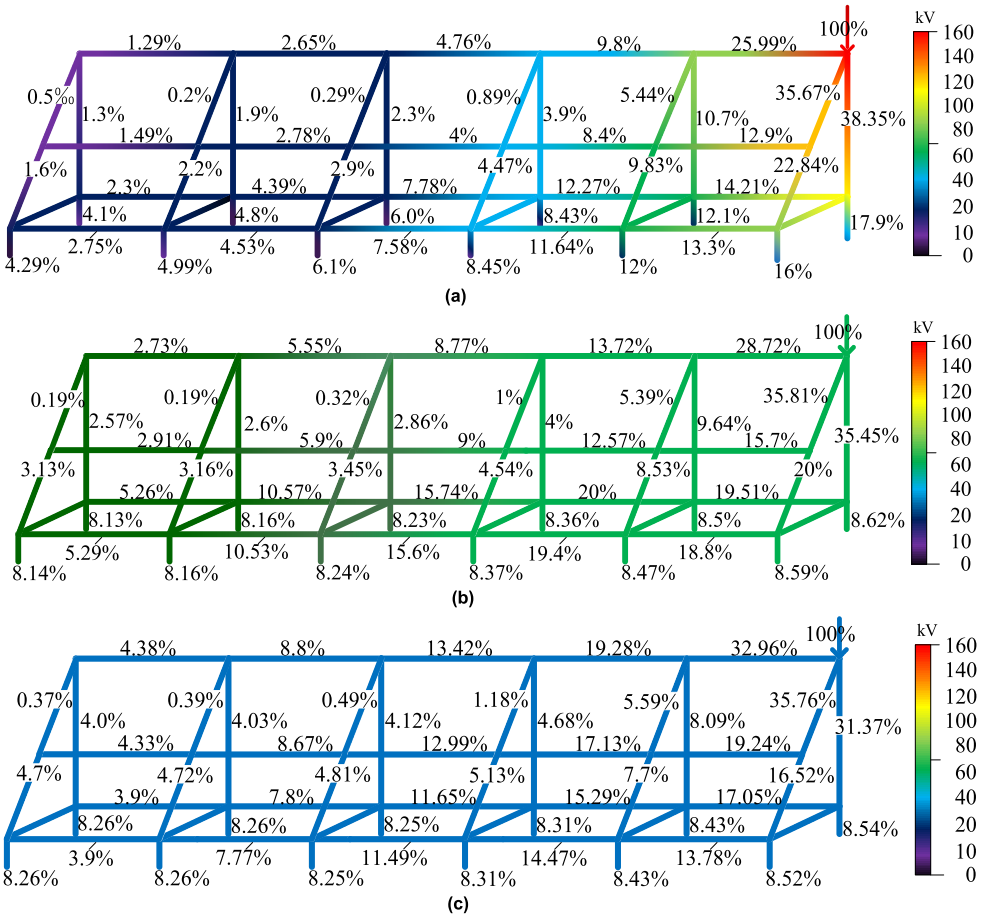

FIGURE 17. Lightning transient distribution on PV bracket structure. (a) 0.55 μs. (b) 10 μs. (c) 350 μs.

the attachment point are still greater than those on other branches.

The potential distributions are also illustrated in Fig. 17 by the color contrast. An excessive distortion appears on the supporting framework at 0.55 μs. The potentials at the positions close to the attachment point are far higher than those distant from attachment point, as shown in Fig. 17(a). The distribution distortion comes to weaken with the potentials distant from attachment point increasing by a small margin at 10 μs, as shown in Fig. 18(b). As the transient process continues for 350 μs, the potential distribution tends to be uniform and various positions approximately assume the same color in the framework [see Fig. 8(c)]. This is due to the fact that various branches progressively take equipotential effect in the framework from 0.55 μs to 350 μs.

Besides the dynamic examination of the lightning transient responses at the three typical instants, the peak values of the currents and potentials are extracted for all the branches and nodes in the supporting framework, since they are widely used in the lightning protection design. Similar to ICF, the peak current factor (PCF) is introduced by the ratio of peak branch current to peak lightning current. The PCFs are marked on various branches in the supporting framework, as shown in Fig. 18(a). Their distribution presents a distortion behavior, i.e. the higher PCFs concentrate on the branches connected to the attachment point. In addition, the peak potentials are also given at various nodes in the supporting framework, as shown in Fig. 18(b), which reveals that the peak potentials at the nodes close to the attachment point are greater than those at other nodes.

It follows from Figs.18-19 that the distribution concentration behavior of the lightning transient responses is obvious in the framework. This will give rise to the high currents and potentials near the attachment point during a lightning stroke and result in severe damages to the solar panels and neighboring installations. Consequently, considerable attention should be paid to the protection against the lightning transient effects near the attachment point.

To investigate the positional influence of the attachment point on the lightning transient responses, the node P4 is also taken as the attachment point (see Fig. 14). The corresponding PCFs and peak potentials are calculated for the supporting framework, as shown in Fig. 19. A contrast between Fig. 18 and Fig. 19 demonstrates that the PCFs and peak potentials near the attachment point P4 is obviously lower than those near the attachment point P1.

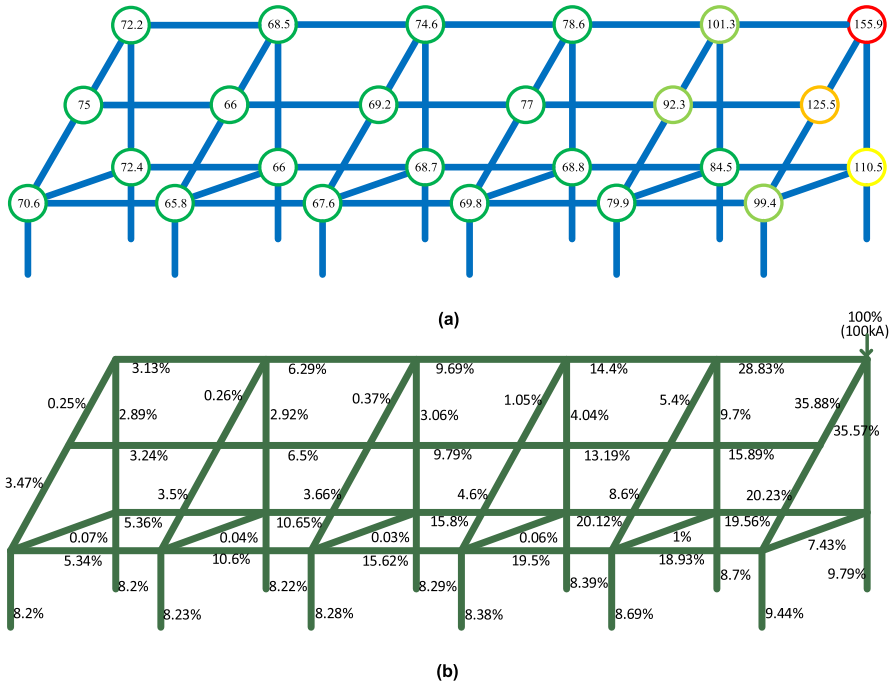

FIGURE 18. Distribution of lightning transient peak responses when impulse injected from P1. (a) Distribution of potential peak values (kV). (b) Distribution of current peak values.

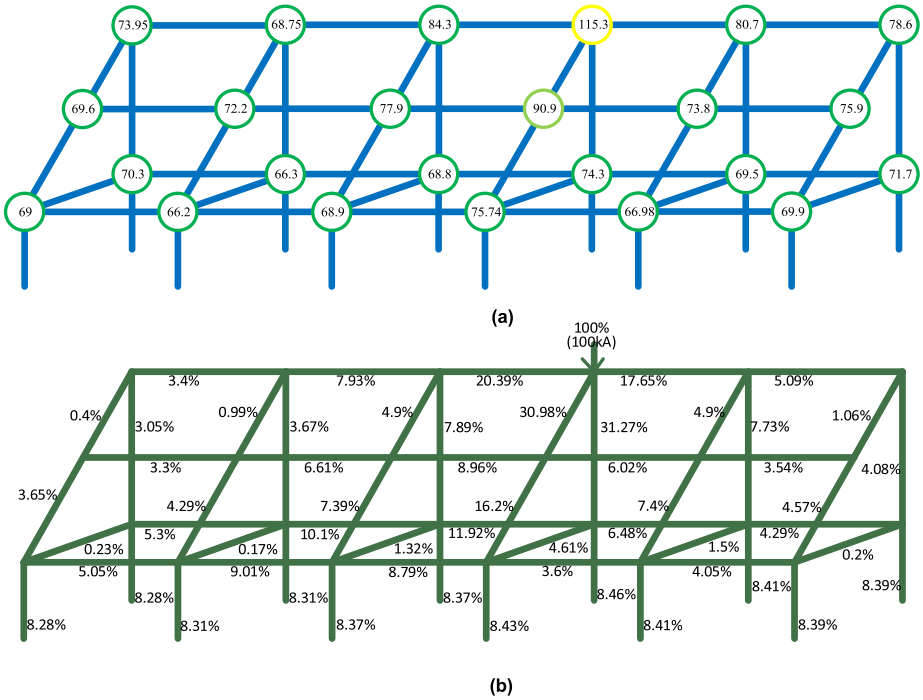

FIGURE 19. Distribution of lightning transient peak responses when impulse injected from P4. (a) Distribution of potential peak values (kV). (b) Distribution of current peak values.

VI. CONCLUSION

An efficient algorithm has been developed for determining the electrical parameters of the conducting branches in the PV bracket system. The algorithm provides a complete set of formulas for evaluating the branch capacitances and inductances and has the capability of taking into account the electromagnetic couplings among the conducting branches in different spatial positions. On the basis of the electrical parameters, the complete circuit model is built for the PV bracket systems. The lightning transient responses in the PV bracket systems are obtained by using the circuit model to carry out the transient calculation. The laboratory experiment

has been made on a reduced-scale bracket system. The comparison between measured and calculated results confirms the validity of the equivalent circuit model. Furthermore, a numerical example has also been provided for an actual bracket system and the distribution behaviour of the lightning transient responses has been investigated in the bracket system. The proposed circuit model is useful in lightning transient analysis of PV bracket systems and can provide a basis for the lightning protection design of PV generation systems.

REFERENCES

[1] N. I. Ahmad *et al.*, "Lightning protection on photovoltaic systems: A review on current and recommended practices," *Renew. Sustain. Energy Rev.*, vol. 82, pp. 1611–1619, Feb. 2017.
[2] C. A. Christodoulou, L. Ekonomou, I. F. Gonos, and N. P. Papanikolaou, "Lightning protection of PV systems," *Energy Syst.*, 2016, vol. 7, no. 3, pp. 469–482, 2016, doi: 10.1007/s12667-015-0176-2.
[3] *Damage Statistic for Solar PV Due to Lightning*. Accessed: May 13, 2016. [Online]. Available: https://www.dehn-international.com
[4] S. Shimura, R. Herrero, M. K. Zuffo, J. Aquiles, and B. Grimoni, "Production costs estimation in photovoltaic power plants using reliability," *Solar Energy*, vol. 133, pp. 294–304, Aug. 2016
[5] C. A. Charalambous, N. D. Kokkinos, and N. Christofides, "External lightning protection and grounding in large-scale photovoltaic applications," *IEEE Trans. Electromagn. Compat.* vol. 56, no. 2, pp. 427–434, Apr. 2014.
[6] C. Dechthummarong, D. Chenvidhya, C. Jivacate, and K. Kirtikara, "Experiment and simulation impulse partial discharge behavior in dielectric encapsulations of field-aged PV modules," in *Proc. IEEE Photovoltaic Spec. Conf.*, Jun. 2011, pp. 003109–003112.
[7] T. Jiang and S. Grzybowski, "Impact of lightning impulse voltage on polycrystalline silicon photovoltaic modules," in *Proc. Int. Symp. Lightning Protection*, 2013, pp. 287–290.
[8] I. Naxakis, E. Pyrgioti, V. Perraki, and E. Tselepis, "Studying the effect of the impulse voltage application on sc-Si PV modules," *Solar Energy*, vol. 144, pp. 721–728, Mar. 2017.
[9] N. H. A. Rahim, Z. A. Baharudin, and M. N. Othman, "Investigation of wave propagation to PV-solar panel due to induced overvoltage generated by lightning impulse generator," *Adv. Sci. Technol. Lett., Energy*, vol. 38, no. 8, pp. 15–22, 2013.
[10] J. C. HernÁndez, P. G. Vidal, and F. Jurado, "Lightning and surge protection in photovoltaic installations," *IEEE Trans. Power Del.*, vol. 23, no. 4, pp. 1961–1971, Oct. 2008.
[11] K. Yamamoto, J. Takami, and N. Okabe, "Overvoltages on DC side of power conditioning system caused by lightning stroke to structure anchoring photovoltaic panels," *Elect. Eng. Jpn.*, vol. 187, no. 4, pp. 29–41, 2014.
[12] X. Zhang and C. Liu, "Lightning transient modeling of wind turbine towers," *Int. Rev. Elect. Eng.*, vol. 7, no. 1, pp. 3505–3611, 2012.
[13] Z. Xiaoqin, *Lightning Protection Design of Wind Turbines*. Beijing, China, Electric Power Press, 2009, p. 151.
[14] A. Ametani, N. Nagaoka, Y. Baba, T. Ohno, and K. Yamabuki, *Power System Transients*. Boca Raton, FL, USA: CRC Press, 2017, pp. 108–115.
[15] U. Y. Iosseli, A. S. Kothanof, and M. G. Stlyrski, *Calculation of Capacitances*. Moscow, Russia, Electric Power Press, 1991.
[16] A. Ametani, Y. Kasai, J. Sawada, A. Mochizuki, and T. Yamada, "Frequency-dependent impedance of vertical conductors and a multiconductor tower model," *IEE Proc.-Gener., Transmiss. Distrib.*, vol. 141, no. 4, pp. 339–345, 1994.
[17] R. B. Standler, *Protection of Electronic Circuits From Overvoltages*. Hoboken, NJ, USA: Wiley, 1989, pp. 68–69.
[18] S. Cristina and A. Orlandi, "Calculation of the induced effects due to a lightning stroke," *IEE Proc. B-Electr. Power Appl.*, vol. 139, no. 4, pp. 374–380, Jul. 1992.
[19] V. Z. Anenkov, "Spark discharge in the soil around the grounding electrodes of a lightning protection system," *Elektrichestvo*, no. 12, pp. 15–20, 1993.
[20] R. Velazquez and D. Mukhedkar, "Analytical modelling of grounding electrodes transient behavior," *IEEE Trans. Power App. Syst.*, vol. PAS-103, no. 6, pp. 1314–1322, Jun. 1984.
[21] G. Celli and F. Pilo, "EMTP models for current distribution evaluation in LPS for high and low buildings," in *Proc. ICLP*, Rhodes, Greece, Jul. 2000, pp. 440–445.
[22] V. A. Rakov *et al.*, "CIGRE technical brochure on lightning parameters for engineering applications," in *Proc. ICLP*, Belo Horizonte, Brazil, Oct. 2013, pp. 373–377.
[23] H. W. Dommel, *Electromagnetic Transients Program Theory Book*. Portland, OR, USA: BPA, 1995, pp. 3–19.
[24] *Protection Against Lightning—Part 1: General Principles*, 2nd ed., document IEC 62305-1, IEC, Geneva, Switzerland, 2010, p. 22.

YAOWU WANG was born in China, in 1988. He received the B.Sc. and master's degrees in electrical engineering from Beijing Jiaotong University, in 2010 and 2015, respectively, where he is currently engaged in research on the electromagnetic transient simulation and lightning protection design of PV systems for his Ph.D. degree.

XIAOQING ZHANG received the M.Sc. and Ph.D. degrees in high voltage engineering from Tsinghua University, Beijing, China, in 1985 and 1990, respectively. Since 1993, he has been with the School of Electrical Engineering, Beijing Jiaotong University, where he is currently a Senior Research Fellow. He has authored six books and more than 50 articles. His research interests include high voltage insulation, lightning protection, and electromagnetic transient simulation.

SHIQI TAO was born in Chaoyang, China, in 1990. He received the B.Sc. degree in electrical engineering from Beijing Jiaotong University, Beijing, China, in 2013, where he is currently pursuing the Ph.D. degree in electrical engineering. His research interests include electromagnetic transients in power systems and lightning protection of wind turbines.